American Mineralogist, Volume 110, pages 1012–1023, 2025

Correlations between the structural and impurity features reveal fluctuant growth conditions of natural fibrous diamonds

Chengyang Sun[1,2,‡], Mingyue He[1,*,†], Taijin Lu[3,*], Shinji Muraishi[2], and Yi Deng[1]

[1]School of Gemology, China University of Geosciences (Beijing), Beijing 100083, China
[2]School of Materials Science and Engineering, Tokyo Institute of Technology, Tokyo 152-8550, Japan
[3]National Gems & Jewelry Co. Ltd., Beijing 100013, China

Abstract

Fibrous diamonds containing mantle fluid inclusions have been studied to explore their unique growth patterns and the evolution of mantle fluids. However, the growth of fibrous diamonds is not a completely homogeneous process, and there has been limited focus on the growth fluctuations of the diamonds themselves. This gap in research hinders our understanding of mantle fluid evolution. To address this issue, polarizing microscope, energy-dispersive spectroscopy (EDS), cathodoluminescence (CL), Raman spectroscopy, and Fourier transform infrared spectroscopy (FTIR) were used to investigate the distribution and composition of fluid micro-inclusions, growth structure, plastic deformation, residual stress, and impurities in coated diamonds from the Democratic Republic of the Congo (DRC). It was found that VN_3H defects controlled the luminescence of diamond growth layers, and plastic deformation and residual stress were mainly related to nitrogen content. However, the relationship between VN_3H defects and nitrogen content in the core varied, leading to contrasting correlations with plastic deformation and residual stress. In the fibrous coat, there are growth layers with varying densities of micro-inclusions. Interestingly, both the dark fibrous layers with the highest density of micro-inclusions and the light-yellow fibrous layers with the lowest density of micro-inclusions showed positive anomalies of plastic deformation, tensile residual stress, nitrogen concentration, and VN_3H defects. According to the micro-inclusion composition and the effect of growth conditions on the growth rate and impurity incorporation of diamonds, it was speculated that growth media with high water contents led to the formation of dark layers with the highest growth rate, and reduced growth pressures were the major reason causing the crystallization of light-yellow fibrous layers. This study demonstrates that the nucleation of natural fibrous diamonds could be subjected to the influence of multiple factors, and the systematic correlations between the structural and impurity features of diamonds have the potential to reflect variations of mantle conditions under which they crystallized.

Keywords: Fibrous diamond, impurity, growth structure, growth condition

Introduction

Diamonds attract geologists' attention because they carry valuable information from deep within the Earth. Due to the extreme growth conditions and superior stabilities of diamonds, their growth structures, impurity features, surface morphologies, and characteristics of trapped inclusions all provide crucial clues about their growth and post-growth history, thus offering us a window into the mantle conditions under which they crystallized (Harris et al. 2022).

Coated diamonds, a type of fibrous diamond, consist of an octahedral monocrystalline core and a fibrous coat. Carbon and nitrogen isotopic studies of the core and coat have revealed that they were formed from different carbon sources (Boyd et al. 1992; Zedgenizov et al. 2020). The significantly higher nitrogen aggregation rate in the core compared to the coat also suggests that they were formed by separate events (Yelisseyev et al. 2004). Numerous fluid inclusions were encapsulated between fibers in the coat during its crystallization (Weiss et al. 2022). Previous studies about fibrous diamonds mainly focused on the compositional features of fluid inclusions to investigate the metasomatic reactions responsible for their special fibrous growth (Kopylova et al. 2010). The composition of fluid inclusions within a single fibrous diamond is not entirely homogeneous. Klein-BenDavid et al. (2004) observed the transformation of brine micro-inclusions into carbonatitic melt, accompanied by a change in the carbon isotopic composition from the inner to outer growth zones of a fibrous diamond from the Diavik mine. Weiss et al. (2009) identified a transition from silicic to carbonatitic fluids toward the rim of fibrous diamonds from Kankan, Guinea. Zedgenizov et al. (2011) reported that the compositions of micro-inclusions in fibrous diamonds from the Ebelyakh placers changed from carbonatitic to silicic. These reports about compositional variations of fluid inclusions within a single fibrous diamond indicate that the growth conditions of fibrous diamonds were not stable. However, most studies about fluid inclusions in fibrous diamonds based on the average composition of a certain amount of tested micro-inclusions have overlooked fluctuations of growth conditions, and few studies have focused on the variation of the diamond itself during the fluctuating growth process.

Fortunately, growth conditions have impacts on various properties of diamonds. The nucleation of natural fibrous diamonds has

* Co-corresponding author E-mails: hemy@cugb.edu.cn, taijinlu@hotmail.com
† Open access: Article available to all readers online.
‡ Orcid https://orcid.org/0000-0002-0105-5690

0003-004X/25/0007–1012$05.00/DOI: https://doi.org/10.2138/am-2024-9503

been attributed to the involvement of increased water content (Smith et al. 2015). With increasing water, the diamond growth rate would increase, and the morphology of grown diamonds evolves from octahedra to {111} dendrites (Palyanov et al. 2012). The diamond growth rate is also influenced by growth temperature and pressure. Experimental results from chemical vapor deposition (CVD) synthesis of diamonds revealed that the growth rate increases with both growth pressure and substrate temperature (Sakaguchi et al. 1999; Brinza et al. 2008; Cao et al. 2021). In high-pressure high-temperature (HPHT) synthesis of diamonds, the diamond growth rate also strongly depends exponentially on temperature (Palyanov et al. 2017). Moreover, growth temperature and pressure can affect the incorporation of N and H atoms into diamonds during growth. For example, Tian et al. (2009) observed a decrease in nitrogen concentration in HPHT diamonds from 460 to 117 ppm with an increase in temperature from 1500 to 1560 K at 5.5 GPa. Liu et al. (2023) reported that nitrogen concentration decreased from 279 to 241 ppm when growth pressure increased from 5.8 to 6.8 GPa at 1600 K. While hydrogen incorporation decreases with increasing pressure (Sakaguchi et al. 1999), and it increases with higher substrate temperatures (Tang et al. 2004). In addition, in polycrystalline diamonds, the incorporation of impurity atoms would also be promoted by decreasing grain size (Xu et al. 2007; Tang et al. 2010; Chen et al. 2023). Therefore, based on the influence of growth conditions on the structural and impurity features of diamonds, changes in growth conditions could be recovered in turn. This study took coated diamonds from the Democratic Republic of the Congo (DRC) as an example, explored correlations between the distribution of micro-inclusions, plastic deformation, residual stress, and impurity defects, and attempted to recover fluctuations of growth conditions responsible for the variation of these features, which strengthened our cognition about the crystallization process of fibrous diamonds, and provided new perspectives to investigate mantle condition evolution responsible for the growth of diamonds.

Materials and Methods

This study examined 70 coated diamonds collected from the DRC through polarizing microscope. The diamonds were cut and polished into smooth sections ~0.3 mm thick. Of all the diamonds examined, 20 samples with prominent color differences in the fibrous coat all showed apparent correlations between structural and impurity features (as summarized in Online Materials[1] Table S1). Two representative sections cut along the (110) planes, labeled DRC196 (3 × 4 mm) and DRC205 (5 × 7 mm), were selected to illustrate the study's findings. The distribution of micro-inclusions and birefringence in the samples was observed using an Olympus BX51 polarizing microscope (the Open Facility Center, Tokyo Institute of Technology, Japan). Both DRC196 and DRC205 exhibited transparent cores surrounded by fibrous coats containing numerous micro-inclusions (Figs. 1a and 1d). The fibrous layers, varying in micro-inclusion density, displayed different colors under single polarized light: dark layers with high density (dashed black rectangles), gray layers with medium density (dashed gray rectangles), and light-yellow layers with low density of micro-inclusions (dashed light-yellow rectangles) (Figs. 1b and 1e). Birefringence patterns are primarily distributed along the boundaries of layers with differing micro-inclusion densities (Figs. 1c and 1f), indicating strong strain between them.

The growth structures of these two samples were revealed through cathodoluminescence (CL) imaging using a ZEISS Sigma 300 scanning electron microscope (SEM) with an accelerating voltage of 10 kV and a working distance of 15 mm (Institute of Mineral Resources, Chinese Academy of Geological Sciences, China). Raman mapping tests conducted on regions indicated by blue rectangles in Figures 1a and 1d, were performed with a Renishaw inVia Raman spectrometer equipped with a Leica DM 2500M microscope in confocal mode. These tests were conducted at room temperature with a step size of 10 μm (Innovation Center, National Gems and Jewelry Co. Ltd., China). Before each test, the spectrometer was calibrated according to the 520.7 cm^{-1} band of a silicon wafer (Kadlečíková et al. 2018). Every spectrum was collected with a static scan from 741.1 to 1880.5 cm^{-1}, using a laser wavelength of 532 nm, a laser power of 5 mW, a grating of 2400 L/mm, an exposure time of 1 s, and an accumulation of 1. The full-width at half maximum (FWHM) of the LO = TO band, which is sensitive to the lattice disorder (Stoneham 1968), was used to indicate the degree of plastic deformation in the diamonds (Erasmus et al. 2011; Agrosì et al. 2017). Due to the effect of stress on changing bond lengths in the diamond lattice, the vibration frequencies of these

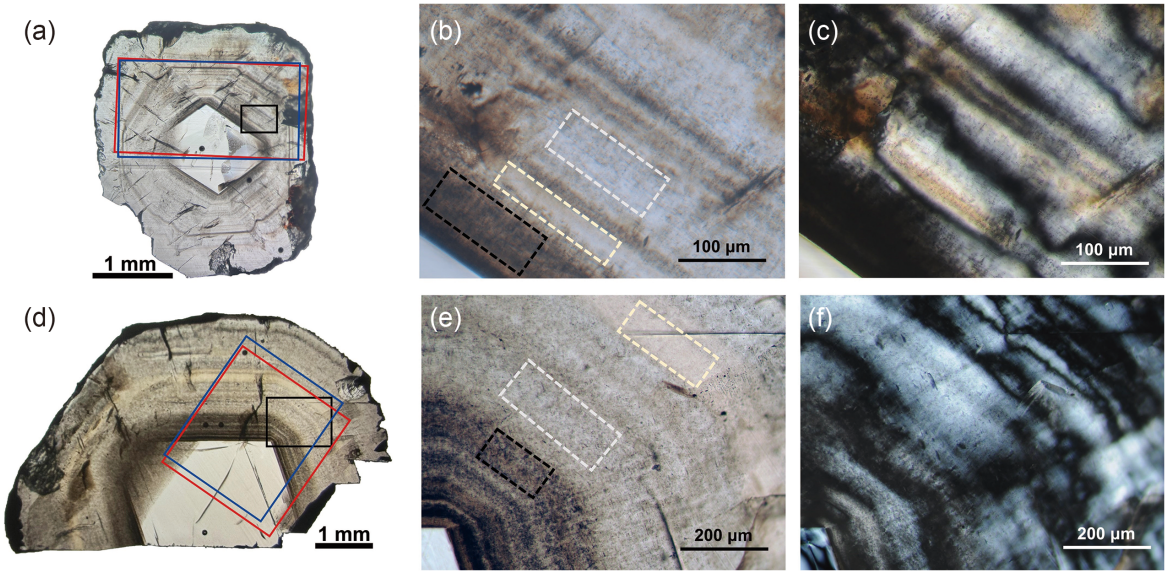

Figure 1. Microscopic images of DRC196 (**a**) and DRC205 (**d**). Blue rectangles indicate the regions of Raman mapping tests, and red rectangles indicate the regions of FTIR mapping tests. (**b**) and (**e**) are single-polarized images of the regions indicated by black rectangles in (**a**) and (**d**), respectively. (**c**) and (**f**) show birefringence patterns of the same region of (**b**) and (**e**), respectively, under cross-polarized light.

bonds together with the Raman shift of LO = TO bands change accordingly. The LO = TO band of an unstressed diamond is featured by the Raman shift of 1332 cm^{-1} and the FWHM of 1.6 cm^{-1}. The peak position shifts to higher wavenumbers with the increase of compressed stress and to lower wavenumbers with the increase of tensile stress (Grimsditch et al. 1978; Izraeli et al. 1999). Therefore, the peak position of the LO = TO bands indicates residual stress in the diamond crystal (Howell et al. 2010). Residual stress in the samples was calculated using the ratios proposed by Grimsditch et al. (1978).

The distribution of impurities in diamonds was determined using micro-Fourier transform infrared spectroscopy (FTIR). FTIR mapping was conducted on regions indicated by red rectangles in Figures 1a and 1d, using a Nicolet iN10 MX micro-FTIR spectrometer equipped with a mercury-cadmium-telluride (MCT) detector and a KBr beam splitter (Innovation Center, National Gems and Jewelry Co. Ltd., China). Samples were placed on a circular CaF_2 plate to collect transmission IR maps with a step size of 50 μm after the detector was cooled to liquid nitrogen temperature. Each spectrum was scanned in the range of 675–4000 cm^{-1} with a spectral resolution of 4 cm^{-1} and an accumulation of 64 scans. After baseline subtraction, normalization, and deconvolution of the absorption spectra, the nitrogen concentration in A centers [N_A, a pair of neighboring substitutional nitrogen atoms (Davies 1976)] and B centers [N_B, four nitrogen atoms surrounding a vacancy (Woods 1986)] were calculated using equations proposed by Boyd et al. (1994, 1995). The H_2O# values [$H_2O/(H_2O+CO_2)$, concentration ratio] were calculated using ratios proposed by Weiss et al. (2010).

The fluid micro-inclusion composition at different positions in the coat of DRC196 and DRC205 was determined using a JED-2300 energy-dispersive spectrometer (EDS) on a JSM-7200F field emission scanning electron microscope (School of Materials Science and Engineering, Tokyo Institute of Technology, Japan). After ultrasonic cleaning with HF (46%) and HNO_3 (60%) acids for two hours, and then rinsing in distilled water and ethanol for an hour, individual micro-inclusions (with size <1 μm) in samples were identified through the lower electron detector imaging (LED, a recombination of low-angle backscattered electrons and secondary electrons) and analyzed using a focused electron beam with an acceleration voltage of 15 keV, a beam current of 14 nA, an acquisition time of 30 s, and ZAF-correction (atomic number, absorption of X-ray emission, and fluorescence) under high-vacuum mode (9.6×10^{-5} Pa). At least 35 micro-inclusions were tested at each position to calculate the average composition.

Results

Growth structures revealed by CL

The cores of coated diamonds exhibited much brighter cathodoluminescence than the coats. Different brightness in the core indicated variations in defects and multi-stage layer growth. The coat was composed of concentric growth layers, with the fibrous layers nearest to the core mimicking its contour and gradually evolving into more cuboid layers toward the rim (Figs. 2a and 2b). CL images revealed no structural transitions between the core and coat. Fibrous crystals oriented perpendicular to the octahedral facets of the core abruptly appeared in the coat (Fig. 2c). Despite the relatively weak luminescence of the coat, the layers within it displayed varying brightness. Comparing CL images with single polarized microscope images, the dark CL layers in the coat corresponded not only to the dark micro-inclusion-rich layers near the core but also to the light-yellow layers with the lowest density of micro-inclusions (Figs. 2a and 2b).

Moreover, the dark layers in the coat did not exhibit apparent fibers, unlike the gray layers (Figs. 2d and 2i). Instead, they featured numerous black triangles smaller than 4 μm under CL (Figs. 2g and 2k). The growth layers in the fibrous coat were jagged, along which there could also be lots of black triangles. The outline of the jagged fibrous growth layer was related to the accumulation of fibers, with the tip of each fiber pointing to a kink of the growth layer (Figs. 2e and 2h). Inside a single fiber, there were straight black lines parallel to the {111} planes, while bright lines existed at the boundaries between fibers, connecting the serrated tips of the jagged growth layers (Figs. 2f and 2h). Additionally, the fibers at the rim of the coat were much longer than those in the inner coat (Fig. 2j).

Distribution of plastic deformation and residual stress

The LO = TO bands of five representative spots at different parts of the two samples are shown in Figures 3a and 3b. These spots were: inner core1, with the highest value of FWHM in the inner core; core rim2, with the lowest FWHM value at the rim of the core; dark coat3, representing the dark growth layer with the highest micro-inclusion density; gray coat4, indicating the gray growth layer with moderate micro-inclusion density; and light-yellow coat5, at the light-yellow layer with the lowest micro-inclusion density. Raman shifts of all these spots were lower than 1332 cm^{-1}, indicating that tensile residual stress dominated in these samples. Moreover, the FWHM of the band increased with the Raman shift's deviation from 1332 cm^{-1}.

Positive anomalies of Raman peak width appeared not only in dark growth layers but also in light-yellow layers (Figs. 3c and 3d). In DRC196, the FWHM of dark and light-yellow layers ranged from 3.5 to 3.9 cm^{-1}, generally higher than that of the gray layers, which ranged from 2.9 to 3.2 cm^{-1}. In DRC205, the FWHM of dark and light-yellow layers ranged from 3.4 to 3.7 cm^{-1}, also higher than that of gray layers, which ranged from 2.9 to 3.1 cm^{-1}. A notable difference between the two samples was the FWHM value of the core. The central core of DRC196 had an FWHM of up to 3.9 cm^{-1}, comparable to the dark fibrous layers in the coat, while the FWHM values of the core of DRC205 (2.19–3.1 cm^{-1}, mostly lower than 2.8 cm^{-1}) were even lower than those of the gray, fibrous layers. Interestingly, both samples showed negative anomalies of FWHM in layers corresponding to the latest growth stage of the core (down to 2.73 cm^{-1} in DRC196 and 2.19 cm^{-1} in DRC205).

The distribution of residual stress in samples is shown in Figures 3e and 3f. In DRC196, residual stress ranged from –0.07 to –0.035 GPa in the core and from –0.39 to 0.11 GPa in the coat. In DRC205, residual stress ranged from –0.05 to –0.25 GPa in the core and from –0.31 to 0.10 GPa in the coat. Positive values indicate compressive stress, while negative values correspond to tensile stress (Nasdala et al. 2004). Both samples predominantly exhibited tensile residual stress throughout the tested regions, with compressive stress appearing only at the fissure tips. Comparing residual stress maps with FWHM maps, it was apparent that regions with stronger plastic deformation (indicated by higher FWHM values) also displayed stronger tensile residual stress.

Impurity distribution and micro-inclusion features

The typical absorption spectra of the inner core1, core rim2, dark coat3, gray coat4, and light-yellow coat5 of the two samples, as indicated by arrows in Figures 4c1 and 4d1, are shown in Figures 4a and 4b. Combined with maps of the distribution of characteristic defects (Figs. 4c and 4d), it was revealed that nitrogen atoms in the core and coat existed in different forms. Nitrogen in the coat existed only in A centers, while the cores contained nitrogen in both A and B centers (Figs. 4c1, 4c2, 4d1, and 4d2). Maps of total nitrogen concentration (N_{total}, Figs. 4c3 and 4d3)

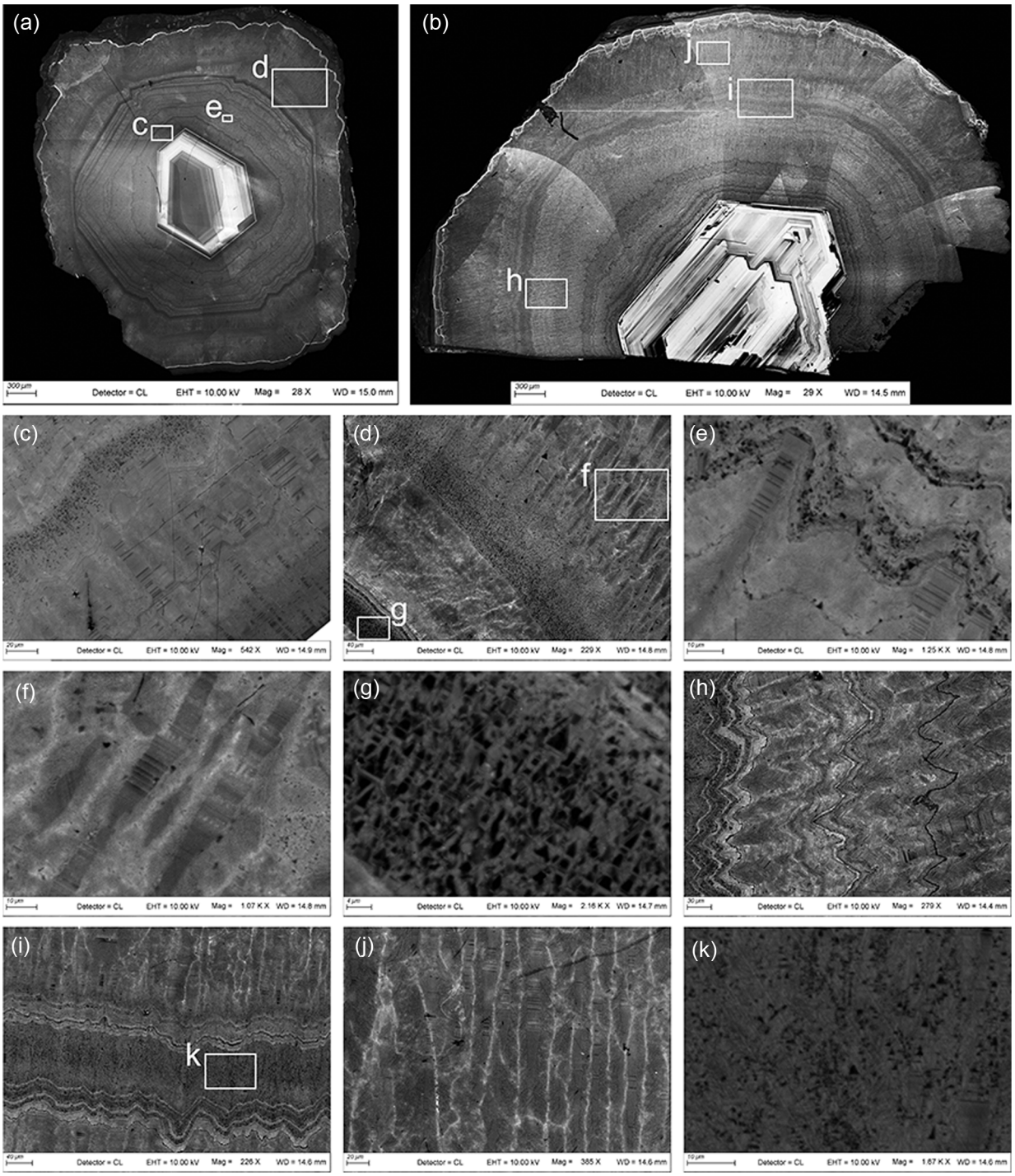

Figure 2. Growth structures of coated diamonds revealed by CL images. The overall CL images of DRC196 (**a**) and DRC205 (**b**). (**c**) Abrupt structure changes from the core to the coat in DRC196. (**d**) Black triangles in dark layers and apparent fibers in gray layers in DRC196. (**e**) Fibers with straight black lines inside them point to kinks of jagged growth layers, along which black triangles also exist. (**f**) Bright lines between fibers in gray layers. (**g**) Black triangles in dark CL layers of DRC196. (**h**) Bright lines between fibers connecting serrated tips of growth layers. (**i**) Dark CL layers with black triangles and gray layers with apparent fibers in DRC205. (**j**) Long fibers at the outermost fibrous growth regions of DRC205, with bright lines between them. (**k**) Black triangles in dark CL layers of DRC205.

showed that in the core, growth layers that crystallized earlier usually had higher N_{total}. At the rim of the core in both samples, there was a sharp decrease in N_A and N_B. The cores also showed absorptions related to platelets (B′, Figs. 4c4 and 4d4); the peak position of platelets in DRC196 was about 1372.21 cm^{-1}, while that in DRC205 was about 1364.37 cm^{-1}. Since the platelet peak

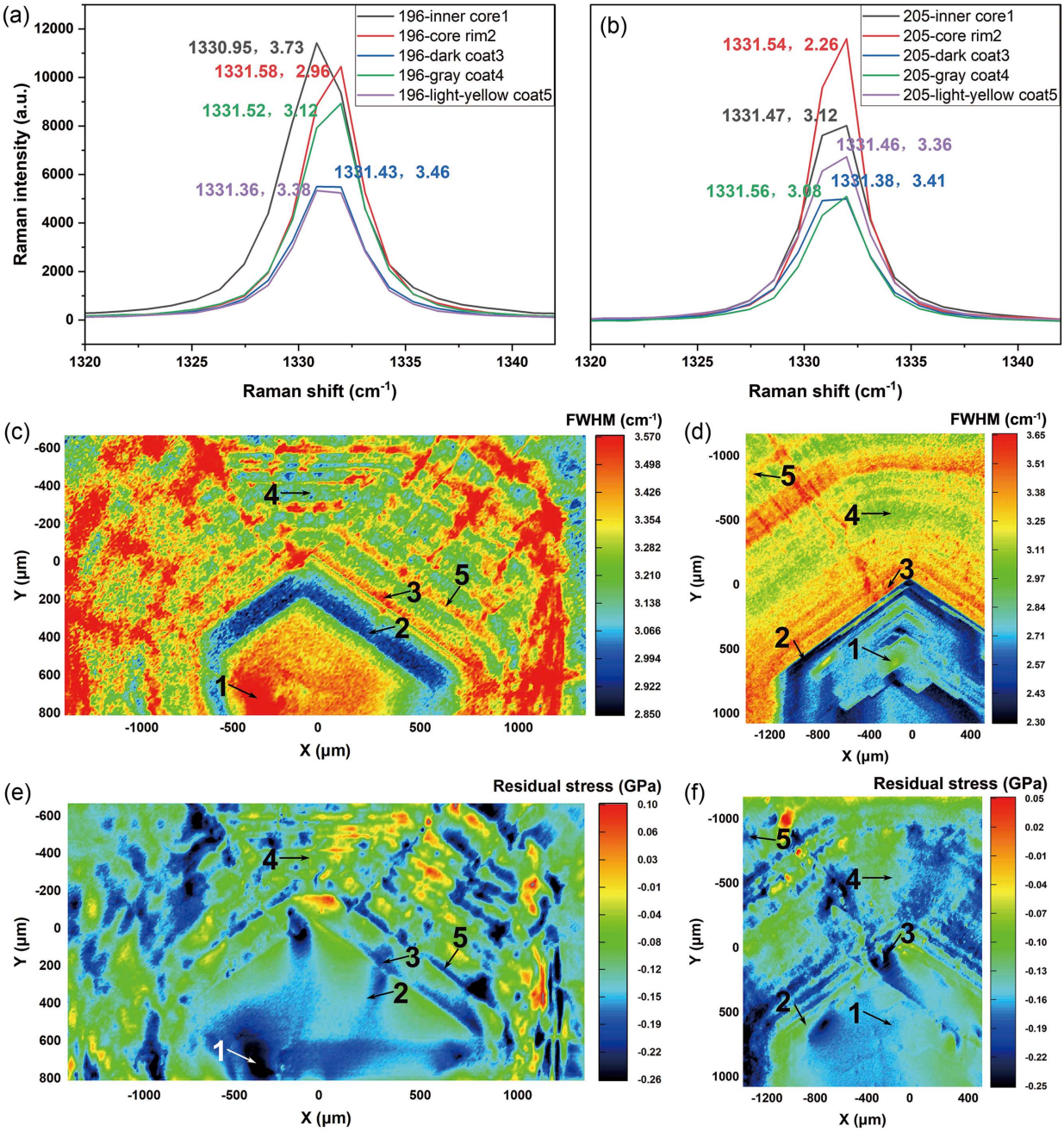

Figure 3. Raman spectra (**a** and **b**), FWHM maps (**c** and **d**), and residual stress maps (**e** and **f**) of DRC196 and DRC205.

position increases as platelet size decreases (Speich et al. 2017), the platelet size in DRC205 was larger than that in DRC196. The absorption coefficients of platelets [μ(B′)] shared very similar distribution features with N_A and N_B in the core. Positive correlations between the concentration of platelets, A centers, and B centers indicated that no significant dissolution of platelets occurred during the annealing (Woods 1986). Regarding the absorption of VN_3H defects [μ(VN_3H), Figs. 4c5 and 4d5], it was apparent that the outer parts of the core displayed very low values of μ(VN_3H) (absorptions lower than 0.4 cm^{-1}), and high values of μ(VN_3H) only occurred in certain parts of the core (up to 1.10 cm^{-1} in the core of DRC196, and 0.95 cm^{-1} in the core of DRC205). In addition, the distribution of VN_3H defects within the core did not correspond with the distribution of nitrogen or platelets. Specifically, in the core of DRC205, regions exhibiting higher nitrogen concentration and μ(B′) showed lower μ(VN_3H) values.

In the fibrous coat, nitrogen existed only in A centers, with the highest nitrogen concentration in the darkest fibrous layers closest to the core, reaching up to 1820 ppm in DRC196 and 1670 ppm in DRC205. The N_A in the outer fibrous parts of DRC196 was

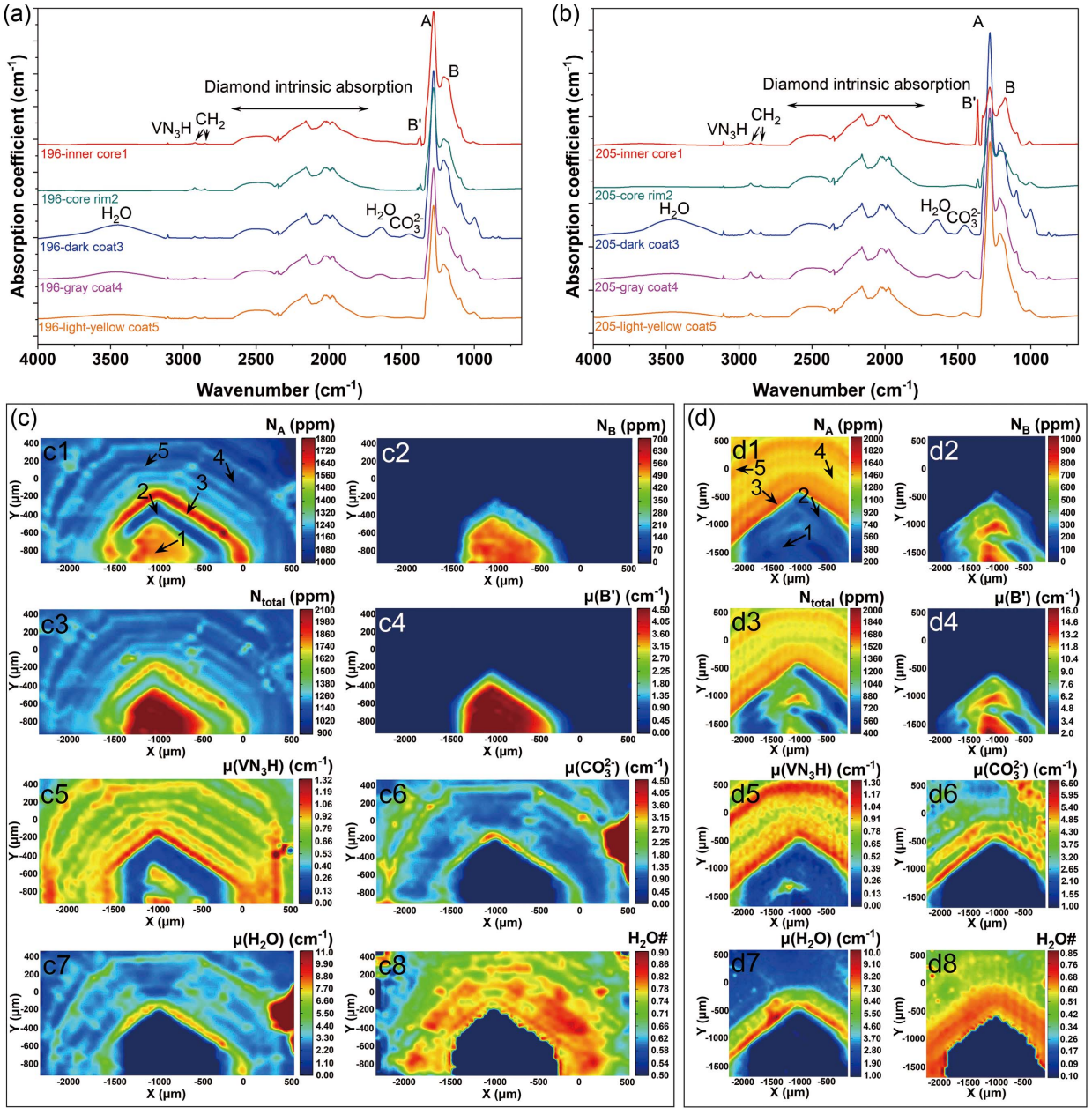

Figure 4. FTIR spectra (**a** and **b**) and distribution maps of various impurities (**c** and **d**) in DRC196 and DRC11205.

typically lower than that of the core, whereas, in DRC205, the N_A in the coat was much higher than that in the core. Both samples demonstrated higher $\mu(VN_3H)$ values in the coats compared to the cores. In fibrous regions, absorptions related to water and carbonates were the highest in dark coat layers, followed by gray coat layers, while light-yellow coat layers displayed the lowest absorptions, consistent with the lowest micro-inclusion density as observed under the microscope (Figs. 1b and 1e). Dark fibrous layers with higher micro-inclusion densities displayed positive anomalies of N_{total} (equivalent to N_A in the fibrous coat), $\mu(VN_3H)$, and absorptions related to carbonates [$\mu(CO_3^{2-})$] and water [$\mu(H_2O)$] (Figs. 4c5–4c7 and 4d5–4d7). However, light-yellow fibrous layers with negative anomalies of $\mu(CO_3^{2-})$ and $\mu(H_2O)$ also displayed positive anomalies of N_{total} and $\mu(VN_3H)$. Moreover, higher absorptions of carbonates and water did not necessarily correspond to higher H_2O# values. Although dark coat layers exhibited the highest H_2O# values, light-yellow fibrous layers could also display positive anomalies of H_2O# (Fig. 4c6–4c8 and 4d6–4d8).

Micro-inclusions in the fibrous coat mainly belonged to silicic or silicic–carbonatitic groups and were enriched in SiO_2, K_2O, CaO, Al_2O_3, FeO, MgO, and Cl. From the inner dark fibrous layers to the outer gray and light-yellow layers, micro-inclusions displayed compositional variations. The SiO_2 contents of

micro-inclusions in the dark layers were the highest, then the micro-inclusions in the light-yellow layers. Micro-inclusions in the gray layers had the lowest content of SiO_2, but the highest content of CaO (Online Materials[1] Table S2).

Discussion

Correlations between structural and impurity features in coated diamonds

Based on the contents above, the distribution of micro-inclusions, growth structures, and characteristics of plastic deformation and residual stress could all be related to the distribution of nitrogen and hydrogen-related defects. In fibrous regions, dark layers with the highest micro-inclusion densities and light-yellow layers with the lowest micro-inclusion densities both exhibited weaker luminescence compared to gray layers with moderate micro-inclusion densities. These layers also displayed positive anomalies of FWHM, tensile residual stress, nitrogen concentration, and VN_3H defects. In the cores, the contrast zonings observed under CL were more closely associated with the distribution of VN_3H defects, and regions with higher absorptions of VN_3H defects were darker under CL. Meanwhile, the distribution of FWHM and residual stress in the core appeared to be more related to the distribution of nitrogen content.

Dependence of CL structures. Cathodoluminescence of diamonds under the excitation of electrons is the result of luminescence recombination of various defects. Contrasting luminescence zonings in diamonds primarily arise from the overlapping emissions of band-A emission (425 nm) related to sp^2 hybridization of dislocations (Takeuchi et al. 2001), H3 centers [503 nm, composed of two nitrogen atoms and a vacancy (Iakoubovskii et al. 2001)], and N3 centers [415 nm, composed of three nitrogen atoms and a vacancy (Boyd et al. 1995)]. H3 centers are mainly formed through the trapping of vacancies by A centers (Collins 1978) or the trapping of single nitrogen atoms by NV centers upon irradiation or plastic deformation (Collins 1980). N3 centers are mainly formed during the aggregation of A centers into B centers (Boyd et al. 1995). They could be formed by the combination of A centers with NV centers, or the combination of H3 centers with single substitutional nitrogen atoms (Vasilev et al. 2021). CL spectra of coated diamonds in previous studies revealed band-A emissions in both the core and coat, with additional peaks of H3 centers in the core (Shimobayashi and Kitamura 2001). The formation of VN_3H defects in diamonds primarily involves the trapping of H atoms by N3 centers and the trapping of A centers by VNH defects (Goss et al. 2014; Lai et al. 2020). H atoms play a crucial role in quenching the aggregation of nitrogen atoms, thereby hindering the formation of luminescent centers in the core (H3 and N3 centers) and the coat (mainly H3 centers) while promoting their transformation into VN_3H defects (Day et al. 2023). Consequently, core regions with fewer VN_3H defects exhibited brighter luminescence, whereas fibrous layers with positive anomalies of VN_3H defects appeared even darker under CL. The corresponding relationship between the enrichment of VN_3H defects and the weakening of luminescence also implied that the black triangles in dark layers under CL should be related to VN_3H defects.

Causes of plastic deformation and residual stress. To determine the major factors causing the broadening and shifting of Raman bands of coated diamonds, FWHM together with residual stress was plotted vs. N_A, N_B, and $\mu(VN_3H)$ in Figures 5a and 5b after unifying coordinates of Raman maps and FTIR maps. Both in the core and coat, FWHM and tensile residual stress increased with nitrogen defects (N_A in the coat and both N_A and N_B in the core), and the slopes of N_A were steeper than that of N_B. However, considering the structures of A centers and B centers, it was speculated that nitrogen atoms in B centers had a stronger influence on these two values. Previous studies have documented the broadening of diamond Raman bands with the increase of nitrogen concentration (Surovtsev and Kupriyanov 2017), boron doping (Ushizawa et al. 1998), and dangling bonds (Fabisiak et al. 1993). In CVD synthetic diamonds, the intrinsic Raman band also broadens with increasing growth rates of the diamond films (Bachmann and Wiechert 1992). The shift to lower frequencies of diamond Raman bands with the increase of nitrogen contents has been observed in HPHT-grown diamonds (Chen et al. 2018) due to the expansion effect of nitrogen on the diamond lattice (Ferrari et al. 2018). In addition, although the FWHM and tensile residual stress in the coat of these two samples were also positively related to $\mu(VN_3H)$, the cores of DRC196 and DRC205 displayed different relationships between the $\mu(VN_3H)$ and FWHM as well as the residual stress. For core layers where $\mu(VN_3H)$ was relatively high (>0.4 cm^{-1}), both FWHM and tensile residual stress increased with $\mu(VN_3H)$. But when $\mu(VN_3H)$ was relatively low (<0.4 cm^{-1}), FWHM and tensile residual stress of the core of DRC196 still increased with the increase of $\mu(VN_3H)$, while those of DRC205 decreased with the increase of $\mu(VN_3H)$. Compared to A centers and B centers, VN_3H defects were much fewer (especially in the core) in these samples, thereby having little influence on FWHM or residual stress. As a result, their relationships with FWHM and residual stress depended on their correlation with nitrogen defects and the influence of nitrogen defects on FWHM and residual stress.

Relationship between nitrogen concentration and VN_3H defects. The cores of DRC196 and DRC205 displayed contrasting correlations between $\mu(VN_3H)$ and the concentration of nitrogen defects (Figs. 5c and 5d). Both samples exhibited positive dependence of $\mu(VN_3H)$ on nitrogen contents in the core when $\mu(VN_3H)$ was higher than 0.4 cm^{-1} (indicated by black dashed lines). While in the range of $\mu(VN_3H)$ <0.4 cm^{-1}, the core of DRC196 with relatively high N_A contents showed a positive correlation between $\mu(VN_3H)$ and the concentration of nitrogen defects, but in the core of DRC205 with relatively high N_B contents, $\mu(VN_3H)$ conventionally decreased with the increase of N_A, N_B, and N_{total}. Although it is debatable whether the intensity of the 3107 cm^{-1} peaks could be used for the quantification of hydrogen content in diamond (Sweeney et al. 1999; Day et al. 2024), previous results still revealed that regions with higher hydrogen contents determined by elastic recoil detection analysis (ERDA) or secondary ion mass spectrometry (SIMS) also showed higher intensities of 3107 cm^{-1} peaks in octahedral or mixed-habit diamonds (Vangu et al. 2023; Kaminsky et al. 2024). Therefore, it was assumed that layers with higher $\mu(VN_3H)$ had higher hydrogen contents within the same growth region. $\mu(VN_3H)$ has been observed to exhibit complex relationships with nitrogen content, showing both positive and negative correlations in different types of diamonds. In synthetic

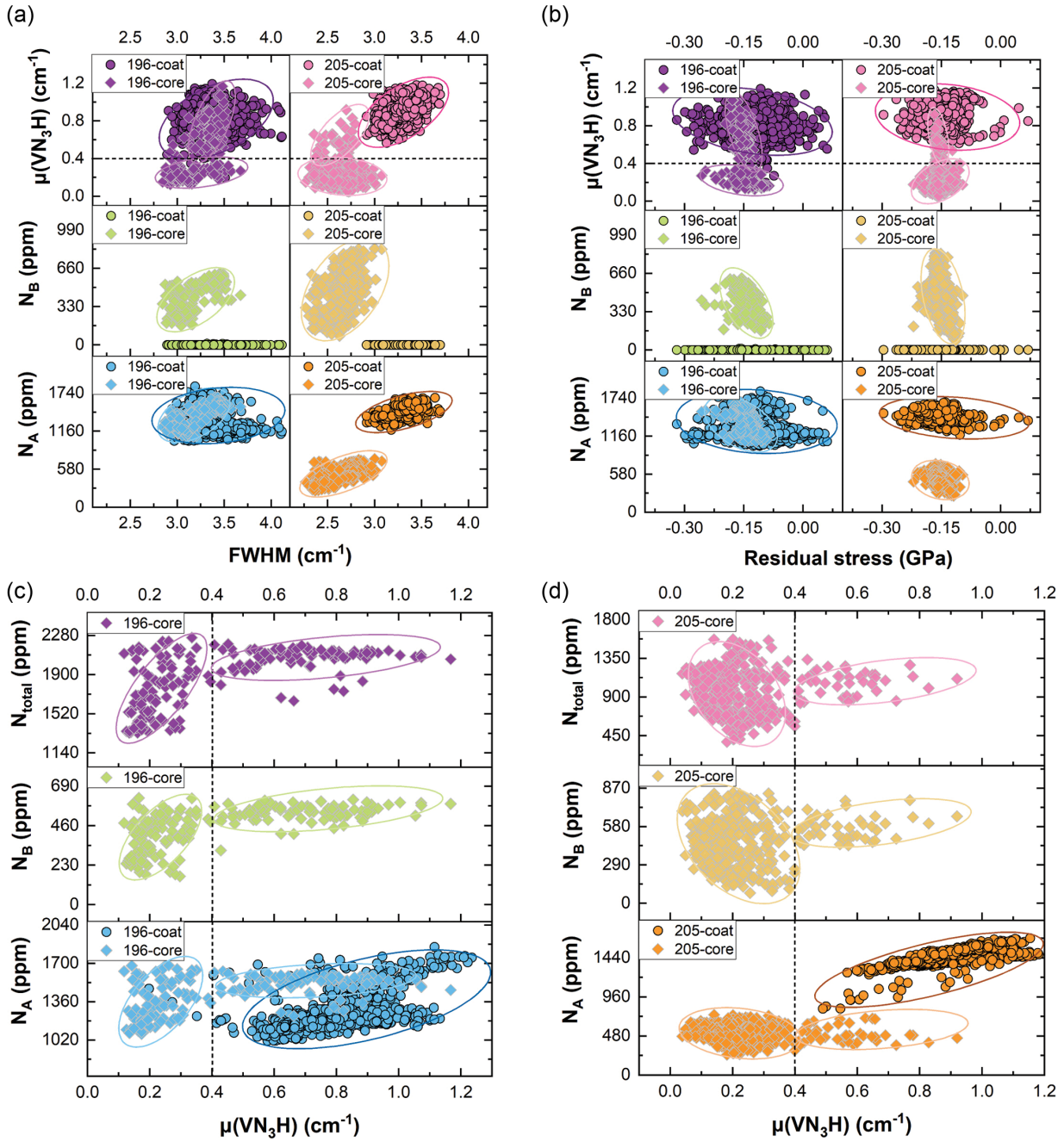

Figure 5. Plots of FWHM (**a**) and residual stress (**b**) vs. N_A, N_B, and $\mu(VN_3H)$, and plots of $\mu(VN_3H)$ vs. N_A, N_B, and N_{total} (**c, d**) in the core and coat of DRC196 and DRC205.

diamonds with a low nitrogen aggregation state, $\mu(VN_3H)$ tends to be positively related to nitrogen content (Kiflawi et al. 1996). Conversely, in natural diamonds with a higher degree of nitrogen aggregation, $\mu(VN_3H)$ is often negatively correlated with N_B (Speich et al. 2017). Mixed-habit diamonds further illustrate this variability, where octahedral sectors with higher nitrogen contents and aggregation states (%IaB = N_B/N_{total}) exhibit lower $\mu(VN_3H)$ compared to cuboid sectors with lower nitrogen contents and aggregation states (Sun et al. 2022). Rondeau et al. (2004) supposed that hydrogen impurities impeded nitrogen aggregation, resulting in higher $\mu(VN_3H)$ but lower aggregation of nitrogen in cuboid sectors. Vasilev et al. (2021) proposed that the inverse dependence of $\mu(VN_3H)$ on B centers was not a directly causal relationship, but resulted collectively from various factors like hydrogen concentration, nitrogen concentration, dislocation density, and micro-inclusion density in different growth sectors. However, few studies about natural diamonds have focused on the statistical relationship between the

concentration of VN_3H defects and nitrogen defects. In this study, even though most of the core of DRC196 did show higher $\mu(VN_3H)$ but lower nitrogen aggregation state compared to the core of DRC205, akin to cuboid sectors compared to octahedral sectors in mixed-habit diamonds, $\mu(VN_3H)$ in the core of DRC196 displayed positive dependence on N_A, N_B, and N_{total} (Fig. 5c). Therefore, it was assumed that when hydrogen content was low [$\mu(VN_3H) < 0.4$ in this study], VN_3H defects in the cores of DRC196 and DRC205 were formed through different processes as a result of distinct annealing conditions.

The significantly lower %IaB values in the core of DRC196 (~30%) compared to DRC205 (~60%) suggested that the core of DRC196 was annealed at lower temperatures or for shorter durations. At relatively low annealing temperatures, under which the formation of B centers was possible, nitrogen atoms in the diamond lattice first aggregated into A centers. With plenty of A centers and a relatively slow aggregation rate of A centers into B centers, A centers would simultaneously contribute to the formation of B centers and VN_3H defects by combining with H3 centers and VNH defects, respectively. This resulted in the positive relationship between $\mu(VN_3H)$, N_A, and N_B, as observed in the core of DRC196. While for the annealing at relatively high temperatures, the aggregation rate of A centers increased. A centers would mainly aggregate into B centers through the formation of N3 centers. However, the formation of VN_3H defects would also occur based on N3 centers (Vasilev et al. 2020). Under this circumstance, nitrogen atoms mainly existed in the form of B centers, but the formation of VN_3H defects impeded the formation of B centers, thus leading to the negative relationship between $\mu(VN_3H)$ and nitrogen contents observed in the core of DRC205. However, with the increase of hydrogen content [i.e., $\mu(VN_3H) > 0.4$ in this study], the formation of VN_3H defects became less dependent on annealing temperature because there was a greater chance for H atoms to be combined with either H3 centers or N3 centers, leading to a slight positive correlation between VN_3H defects and nitrogen concentration. Therefore, considering the positive dependence of FWHM and tensile residual stress on nitrogen concentration, the cores of these samples displayed contrasting correlations of the strength of plastic deformation and tensile residual stress with the content of VN_3H defects. In the coat of these diamonds, where only A centers existed alongside enough high concentration of vacancies and H atoms, VN_3H defects formed through the combination of A centers with VNH defects, resulting in the positive relationship between VN_3H defects and nitrogen defects. In addition, plastic deformation and tensile residual stress were positively related to both nitrogen concentration and VN_3H defects.

Growth condition fluctuations of fibrous diamonds

Over the long residence history, N and H atoms in diamonds have aggregated into more stable forms. However, the aggregation of nitrogen is constrained to a confined volume because nitrogen can only diffuse on a nanometer level (Stachel et al. 2022). The diffusion of hydrogen is faster than nitrogen (Cherniak et al. 2018), but it can still be strongly impeded by point and extended defects (Stacey et al. 2012). Therefore, the distribution of aggregated defects within the fibrous coat has been predetermined since the incorporation of individual N or H atoms during growth. The trapping of nitrogen into the diamond lattice is naturally favored because even a perfect diamond lattice is internally compressed (Dobrinets et al. 2013), and nitrogen could reduce the internal compressive stress by expanding the diamond lattice. Due to the stability change of the diamond lattice under different conditions, the amount of nitrogen incorporated is also growth condition-dependent.

In this study, both dark and light-yellow fibrous layers exhibited elevated nitrogen contents and VN_3H defects (Figs. 6a and 6b). The density of micro-inclusions could be related to the growth rates of diamonds (Howell et al. 2012); the growth rate of dark layers with a high density of micro-inclusions should be higher than that of gray layers, and then light-yellow layers with a low density of micro-inclusions. Fluid micro-inclusions in fibrous diamonds indicate that they crystallized during the interaction between subducted KCl-rich saline fluids and carbonated rocks in the mantle (Weiss et al. 2022). With the increase of water content in the reaction system, produced fluids would be more enriched in SiO_2 and less enriched in CaO (Elazar et al. 2019). This suggests that dark layers crystallized in media with water content higher than those of light-yellow layers, and gray layers were formed in media with relatively low water content. The high growth rate of dark layers could be attributed to the high H_2O# values of the growth medium. Previous HPHT synthesis of diamonds with different water contents demonstrated that water content had an important impact on the diamond morphology (Palyanov et al. 2012). During diamond growth, water not only enhances carbon solubility (Sokol and Pal'yanov 2008) but also lowers the interfacial energy between the diamond surface and growth media (De Yoreo 2003). Consequently, water is expected to promote both fibrous diamond growth and nucleation rates (Smith et al. 2015). Alternatively, the high growth rate of dark layers could result simply from increased carbon supersaturation in the growth medium. High growth rates of dark layers explained their positive anomalies of nitrogen and VN_3H defects because smaller grain sizes under higher growth rates would facilitate stronger incorporation of H atoms into grain boundaries and other structural defects (Michaelson et al. 2007; Tang et al. 2007; Rakha et al. 2009). Moreover, the decrease in grain size would lead to higher compressive stress, thus also promoting the incorporation of nitrogen atoms (Chen et al. 2023). In contrast, light-yellow layers, grown from media with higher H_2O# than gray layers, displayed the lowest growth rates but still showed positive anomalies of nitrogen content and VN_3H defects. Higher nitrogen contents at certain growth layers within a diamond have been attributed to higher nitrogen contents of the growth medium during corresponding growth stages (Zedgenizov et al. 2006). Previous experiments of homoepitaxial diamond growth under different nitrogen doping levels have shown that growth rates first increased with an N_2/CH_4 ratio of up to 20% but decreased with further increases of an N_2/CH_4 ratio of up to 200% (Nakano et al. 2022). Nevertheless, these experiments showed that even with lower growth rates, diamonds grown under N_2/CH_4 ratios higher than 20% still showed higher nitrogen contents. By contrast, the nitrogen contents of light-yellow layers were lower than those of dark layers. Therefore, it was unlikely that light-yellow layers crystallized from growth media with higher nitrogen contents than those of dark layers.

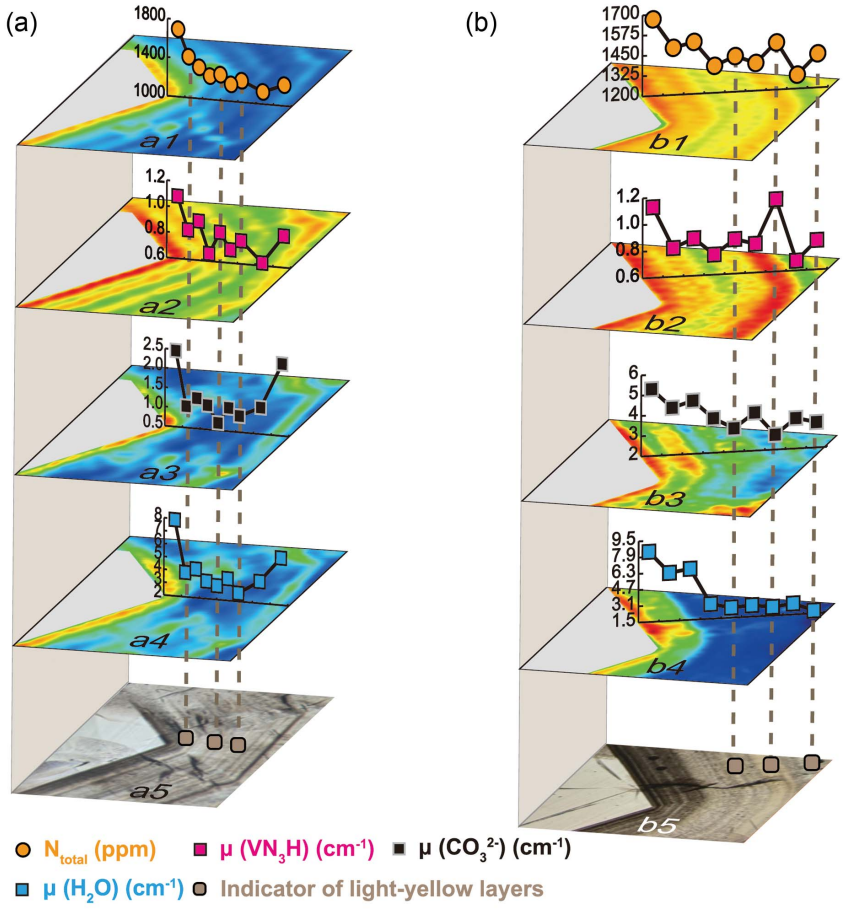

Figure 6. Impurity feature variations during the growth of the coat of DRC196 (**a**) and DRC205 (**b**).

The growth rate and impurity incorporation of diamonds could also be influenced by growth temperature and pressure. Experimental studies on polycrystalline CVD-grown diamonds revealed that growth rates increased with temperatures, pressures, and methane concentrations in the gas phase (Sakaguchi et al. 1999; Brinza et al. 2008; Cao et al. 2021). The decrease in substrate temperature would result in a higher nitrogen concentration in grown diamonds (Lobaev et al. 2017). Similar inverse dependences of nitrogen contents on temperature and pressure were also observed in HPHT diamonds (Tian et al. 2009; Liu et al. 2023). Hydrogen incorporation, on the other hand, increases with growth temperature but decreases with growth pressure (Sakaguchi et al. 1999; Tang et al. 2004). Based on these findings regarding the effects of growth conditions on the growth rate and impurity incorporation, the low growth rate but high content of nitrogen and VN_3H defects in light-yellow layers could result from reduced growth pressure. Additionally, according to the influence of temperature and pressure on nitrogen and hydrogen concentration, the increase in growth temperature or pressure should not be the reason for the high growth rates of dark layers. Therefore, it was speculated that during the growth of the fibrous coat, dark layers grew under higher water contents or higher supersaturation of carbon grew faster, thus incorporating more fluid micro-inclusions, hydrogen, and nitrogen atoms. Although also grown under high water contents, the reduction in growth pressure during the formation of light-yellow layers led to slower growth rates but promoted the incorporation of hydrogen and nitrogen impurities.

Implications

This study has revealed systematic correlations among growth structures, plastic deformation, residual stress, and impurity, as well as micro-inclusion distribution features of coated diamonds from the Democratic Republic of the Congo (DRC). Growth structures observed under CL were related to VN_3H defects, while plastic deformation and residual stress were mainly associated with nitrogen impurities. Nitrogen content in the core could be contrastingly related to VN_3H defects due to different annealing conditions. In the coat, nitrogen contents and VN_3H defects were conventionally positively correlated. However, positive anomalies of nitrogen and VN_3H contents appeared not only at dark fibrous layers with high micro-inclusion densities but also at light-yellow layers with low micro-inclusion densities. Considering factors influencing growth rates and the incorporation of nitrogen and hydrogen atoms during diamond growth, it was speculated that high water contents of growth mediums led to the formation of dark layers, and growth pressure decreases

should be the major reason causing the formation of micro-inclusion-poor but nitrogen- and hydrogen-rich light-yellow fibrous layers. This study advanced our understanding of the unique fibrous growth of natural diamonds and exemplified the occurrence of multiple fluctuations in growth conditions during the rapid crystallization of diamonds. Therefore, careful attention should be paid to the layer position of analyzed micro-inclusions when investigating the compositions of mantle fluids trapped in fibrous diamonds, as fluid inclusions within the same fibrous diamond may form under different conditions. Furthermore, this study suggested that comprehensive investigations into the impurity evolution of diamonds would provide important supplemental information about the evolving mantle conditions in which they crystallized.

Acknowledgments and Funding

This research has been supported by the National Infrastructure of Mineral, Rock and Fossil Resources (grant K1603901); the National Science Foundation of China (grant 42073008); the scientific research program of National Gems & Jewelry Testing Co. Ltd. (grant NGTC20220400), and the program of China Scholarship Council (grant 202306400061).

Masaru Tada (the Open Facility Center, Tokyo Institute of Technology) is acknowledged for allowing the use of the polarizing microscope. The authors also warmly thank Oliver Tschauner and an anonymous reviewer for their constructive comments.

References Cited

Agrosì, G., Tempesta, G., Della Ventura, G., Cestelli Guidi, M., Hutchison, M., Nimis, P., and Nestola, F. (2017) Non-destructive in situ study of plastic deformations in diamonds: X-ray diffraction topography and μFTIR mapping of two super deep diamond crystals from São Luiz (Juina, Brazil). Crystals, 7, 233, https://doi.org/10.3390/cryst7080233.

Bachmann, P.K. and Wiechert, D.U. (1992) Optical characterization of diamond. Diamond and Related Materials, 1, 422–433, https://doi.org/10.1016/0925-9635(92)90141-A.

Boyd, S.R., Pillinger, C.T., Milledge, H.J., Mendelssohn, M.J., and Seal, M. (1992) C and N isotopic composition and the infrared absorption spectra of coated diamonds: Evidence for the regional uniformity of CO_2-H_2O rich fluids in lithospheric mantle. Earth and Planetary Science Letters, 109, 633–644, https://doi.org/10.1016/0012-821X(92)90121-B.

Boyd, S.R., Kiflawi, I., and Woods, G.S. (1994) The relationship between infrared absorption and the A defect concentration in diamond. Philosophical Magazine B, 69, 1149–1153, https://doi.org/10.1080/01418639408240185.

——— (1995) Infrared absorption by the B nitrogen aggregate in diamond. Philosophical Magazine B, 72, 351–361, https://doi.org/10.1080/13642819508239089.

Brinza, O., Achard, J., Silva, F., Bonnin, X., Barroy, P., Corte, K.D., and Gicquel, A. (2008) Dependence of CVD diamond growth rate on substrate orientation as a function of process parameters in the high microwave power density regime. Physica status solidi (a), 205, 2114–2120.

Cao, W., Gao, D., Zhao, H., and Ma, Z. (2021) Epitaxial lateral growth of single-crystal diamond under high pressure by a plate-to-plate MPCVD. Functional Diamond, 1, 143–149, https://doi.org/10.1080/26941112.2021.1947750.

Chen, L., Miao, X., Ma, H., Guo, L., Wang, Z., Yang, Z., Fang, C., and Jia, X. (2018) Synthesis and characterization of diamonds with different nitrogen concentrations under high pressure and high temperature conditions. CrystEngComm, 20, 7164–7169, https://doi.org/10.1039/C8CE01533C.

Chen, K., Tao, T., Hu, W., Ye, Y., Zheng, K., Ye, J., Zhi, T., Wang, X., Liu, B., and Zhang, R. (2023) High-speed growth of high-quality polycrystalline diamond films by MPCVD. Carbon Letters, 33, 2003–2010, https://doi.org/10.1007/s42823-023-00534-y.

Cherniak, D.J., Watson, E.B., Meunier, V., and Kharche, N. (2018) Diffusion of helium, hydrogen and deuterium in diamond: Experiment, theory and geochemical applications. Geochimica et Cosmochimica Acta, 232, 206–224, https://doi.org/10.1016/j.gca.2018.04.029.

Collins, A.T. (1978) Migration of nitrogen in electron-irradiated type Ib diamond. Journal of Physics C: Solid State Physics, 11, L417–L422, https://doi.org/10.1088/0022-3719/11/10/002.

——— (1980) Vacancy enhanced aggregation of nitrogen in diamond. Journal of Physics C: Solid State Physics, 13, 2641–2650, https://doi.org/10.1088/0022-3719/13/14/006.

Davies, G. (1976) The A nitrogen aggregate in diamond-its symmetry and possible structure. Journal of Physics C: Solid State Physics, 9, L537–L542, https://doi.org/10.1088/0022-3719/9/19/005.

Day, M.C., Pamato, M.G., Novella, D., and Nestola, F. (2023) Imperfections in natural diamond: The key to understanding diamond genesis and the mantle. La Rivista del Nuovo Cimento della Società Italiana di Fisica, 46, 381–471, https://doi.org/10.1007/s40766-023-00045-6.

Day, M.C., Jollands, M.C., Novella, D., Nestola, F., Dovesi, R., and Pamato, M.G. (2024) Hydrogen-related defects in diamond: A comparison between observed and calculated FTIR spectra. Diamond and Related Materials, 143, 110866, https://doi.org/10.1016/j.diamond.2024.110866.

De Yoreo, J.J. (2003) Principles of crystal nucleation and growth. Reviews in Mineralogy and Geochemistry, 54, 57–93, https://doi.org/10.2113/0540057.

Dobrinets, I.A., Vins, V.G., and Zaitsev, A.M. (2013) HPHT-Treated Diamonds: Diamonds Forever Vol. 181, 276 p. Springer.

Elazar, O., Frost, D., Navon, O., and Kessel, R. (2019) Melting of H_2O and CO_2-bearing eclogite at 4–6 GPa and 900–1200 °C: Implications for the generation of diamond-forming fluids. Geochimica et Cosmochimica Acta, 255, 69–87, https://doi.org/10.1016/j.gca.2019.03.025.

Erasmus, R.M., Daniel, R.D., and Comins, J.D. (2011) Three-dimensional mapping of stresses in plastically deformed diamond using micro-Raman and photoluminescence spectroscopy. Journal of Applied Physics, 109, 013527, https://doi.org/10.1063/1.3531548.

Fabisiak, K., Maar-Stumm, M., and Blank, E. (1993) Defects in chemically vapour-deposited diamond films studied by electron spin resonance and Raman spectroscopy. Diamond and Related Materials, 2, 722–727, https://doi.org/10.1016/0925-9635(93)90211-J.

Ferrari, A.M., Salustro, S., Gentile, F.S., Mackrodt, W.C., and Dovesi, R. (2018) Substitutional nitrogen in diamond: A quantum mechanical investigation of the electronic and spectroscopic properties. Carbon, 134, 354–365, https://doi.org/10.1016/j.carbon.2018.03.091.

Goss, J.P., Briddon, P.R., Hill, V., Jones, R., and Rayson, M.J. (2014) Identification of the structure of the 3107 cm^{-1} H-related defect in diamond. Journal of Physics: Condensed Matter, 26, 145801, https://doi.org/10.1088/0953-8984/26/14/145801.

Grimsditch, M.H., Anastassakis, E., and Cardona, M. (1978) Effect of uniaxial stress on the zone-center optical phonon of diamond. Physical Review B: Condensed Matter, 18, 901–904, https://doi.org/10.1103/PhysRevB.18.901.

Harris, J.W., Smit, K.V., Fedortchouk, Y., and Moore, M. (2022) Morphology of monocrystalline diamond and its inclusions. Reviews in Mineralogy and Geochemistry, 88, 119–166, https://doi.org/10.2138/rmg.2022.88.02.

Howell, D., Wood, I.G., Dobson, D.P., Jones, A.P., Nasdala, L., and Harris, J.W. (2010) Quantifying strain birefringence halos around inclusions in diamond. Contributions to Mineralogy and Petrology, 160, 705–717, https://doi.org/10.1007/s00410-010-0503-5.

Howell, D., O'Neill, C.J., Grant, K.J., Griffin, W.L., Pearson, N.J., and O'Reilly, S.Y. (2012) μ-FTIR mapping: Distribution of impurities in different types of diamond growth. Diamond and Related Materials, 29, 29–36, https://doi.org/10.1016/j.diamond.2012.06.003.

Iakoubovskii, K., Adriaenssens, G.J., Dogadkin, N.N., and Shiryaev, A.A. (2001) Optical characterization of some irradiation-induced centers in diamond. Diamond and Related Materials, 10, 18–26, https://doi.org/10.1016/S0925-9635(00)00361-7.

Izraeli, E.S., Harris, J.W., and Navon, O. (1999) Raman barometry of diamond formation. Earth and Planetary Science Letters, 173, 351–360, https://doi.org/10.1016/S0012-821X(99)00235-6.

Kadlečíková, M., Breza, J., Vančo, Ľ., Mikolášek, M., Hubeňák, M., Racko, J., and Greguš, J. (2018) Raman spectroscopy of porous silicon substrates. Optik (Stuttgart), 174, 347–353, https://doi.org/10.1016/j.ijleo.2018.08.084.

Kaminsky, F.V., Polyakov, V.B., Ber, B.Ya., Kazantsev, D.Yu., Khachatryan, G.K., and Shilobreeva, S.N. (2024) Hydrogen in natural diamond: Quantification of N3VH defects using SIMS and FTIR data. Chemical Geology, 661, 122185, https://doi.org/10.1016/j.chemgeo.2024.122185.

Kiflawi, I., Fisher, D., Kanda, H., and Sittas, G. (1996) The creation of the 3107 cm^{-1} hydrogen absorption peak in synthetic diamond single crystals. Diamond and Related Materials, 5, 1516–1518, https://doi.org/10.1016/S0925-9635(96)00568-7.

Klein-BenDavid, O., Izraeli, E.S., Hauri, E., and Navon, O. (2004) Mantle fluid evolution—A tale of one diamond. Lithos, 77, 243–253, https://doi.org/10.1016/j.lithos.2004.04.003.

Kopylova, M., Navon, O., Dubrovinsky, L., and Khachatryan, G. (2010) Carbonatitic mineralogy of natural diamond-forming fluids. Earth and Planetary Science Letters, 291, 126–137, https://doi.org/10.1016/j.epsl.2009.12.056.

Lai, M.Y., Breeding, C.M., Stachel, T., and Stern, R.A. (2020) Spectroscopic features of natural and HPHT-treated yellow diamonds. Diamond and Related Materials, 101, 107642, https://doi.org/10.1016/j.diamond.2019.107642.

Liu, Y., Wang, Z., Li, B., Zhao, H., Wang, S., Chen, L., Ma, H., and Jia, X. (2023) Diamond growth in a high temperature and high pressure Fe-Ni-C-Si system: Effect of synthesis pressure. Chinese Physics B, 32, 128102, https://doi.org/10.1088/1674-1056/acf03d.

Lobaev, M.A., Gorbachev, A.M., Bogdanov, S.A., Vikharev, A.L., Radishev, D.B., Isaev, V.A., Chernov, V.V., and Drozdov, M.N. (2017) Influence of CVD diamond growth conditions on nitrogen incorporation. Diamond and Related Materials, 72, 1–6, https://doi.org/10.1016/j.diamond.2016.12.011.

Michaelson, Sh., Lifshitz, Y., Ternyak, O., Akhvlediani, R., and Hoffman, A. (2007) Hydrogen incorporation in diamond films. Diamond and Related Materials, 16, 845–850, https://doi.org/10.1016/j.diamond.2006.11.080.

Nakano, Y., Zhang, X., Kobayashi, K., Matsumoto, T., Inokuma, T., Yamasaki, S., Nebel, C.E., and Tokuda, N. (2022) Impact of nitrogen doping on homoepitaxial diamond (111) growth. Diamond and Related Materials, 125, 108997, https://doi.org/10.1016/j.diamond.2022.108997.

Nasdala, L., Brenker, F.E., Glinnemann, J., Hofmeister, W., Gasparik, T., Harris, J.W., Stachel, T., and Reese, I. (2004) Spectroscopic 2D-tomography : Residual pressure and strain around mineral inclusions in diamonds. European Journal of Mineralogy, 15, 931–935, https://doi.org/10.1127/0935-1221/2003/0015-0931.

Palyanov, Y.N., Borzdov, Y.M., Kupriyanov, I.N., and Khokhryakov, A.F. (2012) Effect of H_2O on diamond crystal growth in metal-carbon systems. Crystal Growth & Design, 12, 5571–5578, https://doi.org/10.1021/cg301111g.

Palyanov, Y.N., Kupriyanov, I.N., Khokhryakov, A.F., and Borzdov, Y.M. (2017) High-pressure crystallization and properties of diamond from magnesium-based catalysts. CrystEngComm, 19, 4459–4475, https://doi.org/10.1039/C7CE01083D.

Rakha, S.A., Jianqing, C., Huihao, X., Guojun, Y., Zhu, D., and Gong, J. (2009) Incorporation of hydrogen in diamond thin films. Diamond and Related Materials, 18, 1247–1252, https://doi.org/10.1016/j.diamond.2009.04.009.

Rondeau, B., Fritsch, E., Guiraud, M., Chalain, J.-P., and Notari, F. (2004) Three historical 'asteriated' hydrogen-rich diamonds: Growth history and sector-dependent impurity incorporation. Diamond and Related Materials, 13, 1658–1673, https://doi.org/10.1016/j.diamond.2004.02.002.

Sakaguchi, I., Nishitani-Gamo, M., Loh, K.P., Haneda, H., and Ando, T. (1999) Homoepitaxial growth and hydrogen incorporation on the chemical vapor deposited (111) diamond. Journal of Applied Physics, 86, 1306–1310, https://doi.org/10.1063/1.370886.

Shimobayashi, N. and Kitamura, M. (2001) Growth habit of needle crystals in coats of coated diamonds. Journal of Mineralogical and Petrological Sciences, 96, 188–196, https://doi.org/10.2465/jmps.96.188.

Smith, E.M., Kopylova, M.G., Frezzotti, M.L., and Afanasiev, V.P. (2015) Fluid inclusions in Ebelyakh diamonds: Evidence of CO_2 liberation in eclogite and the effect of H_2O on diamond habit. Lithos, 216-217, 106–117, https://doi.org/10.1016/j.lithos.2014.12.010.

Sokol, A.G. and Pal'yanov, Yu.N. (2008) Diamond formation in the system MgO-SiO_2-H_2O-C at 7.5 GPa and 1,600 °C. Contributions to Mineralogy and Petrology, 155, 33–43, https://doi.org/10.1007/s00410-007-0221-9.

Speich, L., Kohn, S.C., Wirth, R., Bulanova, G.P., and Smith, C.B. (2017) The relationship between platelet size and the B′ infrared peak of natural diamonds revisited. Lithos, 278-281, 419–426, https://doi.org/10.1016/j.lithos.2017.02.010.

Stacey, A., Karle, T.J., McGuinness, L.P., Gibson, B.C., Ganesan, K., Tomljenovic Hanic, S., Greentree, A.D., Hoffman, A., Beausoleil, R.G., and Prawer, S. (2012) Depletion of nitrogen vacancy color centers in diamond via hydrogen passivation. Applied Physics Letters, 100, 071902, https://doi.org/10.1063/1.3684612.

Stachel, T., Cartigny, P., Chacko, T., and Pearson, D.G. (2022) Carbon and nitrogen in mantle-derived diamonds. Reviews in Mineralogy and Geochemistry, 88, 809–875, https://doi.org/10.2138/rmg.2022.88.15.

Stoneham, A.M. (1968) The shapes of inhomogeneously broadened resonance lines II. Second-order effects. Journal of Physics C: Solid State Physics, 1, 565–574, https://doi.org/10.1088/0022-3719/1/3/302.

Sun, C., Lu, T., He, M., Song, Z., and Deng, Y. (2022) Corresponding relationship between characteristic birefringence, strain, and impurities in Zimbabwean mixed-habit diamonds revealed by mapping techniques. European Journal of Mineralogy, 34, 539–547, https://doi.org/10.5194/ejm-34-539-2022.

Surovtsev, N.V. and Kupriyanov, I.N. (2017) Effect of nitrogen impurities on the Raman line width in diamond, Revisited. Crystals, 7, 239, https://doi.org/10.3390/cryst7080239.

Sweeney, R.J., Prozesky, V.M., Viljoen, K.S., and Connell, S. (1999) The sensitive determination of H in diamond by infrared (FTIR) spectroscopy and micro-elastic-recoil (μ-ERDA) techniques. Nuclear Instruments and Methods in Physics Research: Section B, Beam Interactions with Materials and Atoms, 158, 582–587, https://doi.org/10.1016/S0168-583X(99)00367-5.

Takeuchi, D., Watanabe, H., Yamanaka, S., Okushi, H., Sawada, H., Ichinose, H., Sekiguchi, T., and Kajimura, K. (2001) Origin of band-*A* emission in diamond thin films. Physical Review B, 63, 245328, https://doi.org/10.1103/PhysRevB.63.245328.

Tang, C.J., Neves, A.J., and Fernandes, A.J.S. (2004) Study the effect of O_2 addition on hydrogen incorporation in CVD diamond. Diamond and Related Materials, 13, 203–208, https://doi.org/10.1016/j.diamond.2003.10.032.

Tang, C.J., Neto, M.A., Soares, M.J., Fernandes, A.J.S., Neves, A.J., and Grácio, J. (2007) A comparison study of hydrogen incorporation among nanocrystalline, microcrystalline and polycrystalline diamond films grown by chemical vapor deposition. Thin Solid Films, 515, 3539–3546, https://doi.org/10.1016/j.tsf.2006.10.132.

Tang, C.J., Abe, I., Vieira, L.G., Soares, M.J., Grácio, J., and Pinto, J.L. (2010) Investigation of nitrogen addition on hydrogen incorporation in CVD diamond films from polycrystalline to nanocrystalline. Diamond and Related Materials, 19, 404–408, https://doi.org/10.1016/j.diamond.2010.01.030.

Tian, Y., Jia, X., Zang, C., Li, S., Xiao, H., Zhang, Y., Huang, G., Li, R., Han, Q., Ma, L., and others. (2009) Dependence of nitrogen concentration in type Ib diamonds on synthesis temperature. Science Bulletin, 54, 1459–1462, https://doi.org/10.1007/s11434-009-0211-6.

Ushizawa, K., Watanabe, K., Ando, T., Sakaguchi, I., Nishitani-Gamo, M., Sato, Y., and Kanda, H. (1998) Boron concentration dependence of Raman spectra on {100} and {111} facets of B-doped CVD diamond. Diamond and Related Materials, 7, 1719–1722, https://doi.org/10.1016/S0925-9635(98)00296-9.

Vangu, D., Bureau, H., Khodja, H., Charrondiere, M., Esteve, I., Béneut, K., Remusat, L., Gaillou, E., Cartigny, P., and Bouillard, J.-C. (2023) Combination of ERDA, FTIR spectroscopy and NanoSIMS for the characterization of hydrogen incorporation in natural diamonds. Diamond and Related Materials, 136, 110007, https://doi.org/10.1016/j.diamond.2023.110007.

Vasilev, E.A., Zedgenizov, D.A., and Klepikov, I.V. (2020) The enigma of cuboid diamonds: The causes of inverse distribution of optical centers within the growth zones. Journal of Geosciences, 65, 59–70, https://doi.org/10.3190/jgeosci.301.

Vasilev, E., Zedgenizov, D., Zamyatin, D., Klepikov, I., and Antonov, A. (2021) Cathodoluminescence of diamond: Features of visualization. Crystals, 11, 1522, https://doi.org/10.3390/cryst11121522.

Weiss, Y., Kessel, R., Griffin, W.L., Kiflawi, I., Klein-BenDavid, O., Bell, D.R., Harris, J.W., and Navon, O. (2009) A new model for the evolution of diamond-forming fluids: Evidence from microinclusion-bearing diamonds from Kankan, Guinea. Lithos, 112, 660–674, https://doi.org/10.1016/j.lithos.2009.05.038.

Weiss, Y., Kiflawi, I., and Navon, O. (2010) IR spectroscopy: Quantitative determination of the mineralogy and bulk composition of fluid microinclusions in diamonds. Chemical Geology, 275, 26–34, https://doi.org/10.1016/j.chemgeo.2010.04.010.

Weiss, Y., Czas, J., and Navon, O. (2022) Fluid inclusions in fibrous diamonds. Reviews in Mineralogy and Geochemistry, 88, 475–532, https://doi.org/10.2138/rmg.2022.88.09.

Woods, G.S. (1986) Platelets and the infrared absorption of type Ia diamonds. Proceedings of the Royal Society of London A, 407, 219–238, https://doi.org/10.1098/rspa.1986.0094.

Xu, Z., Lev, L., Lukitsch, M., and Kumar, A. (2007) Analysis of residual stresses in diamond coatings deposited on cemented tungsten carbide substrates. Journal of Materials Research, 22, 1012–1017, https://doi.org/10.1557/jmr.2007.0120.

Yelisseyev, A.P., Pokhilenko, N.P., Steeds, J.W., Zedgenizov, D.A., and Afanasiev, V.P. (2004) Features of coated diamonds from the Snap Lake/King Lake kimberlite dyke, Slave craton, Canada, as revealed by optical topography. Lithos, 77, 83–97, https://doi.org/10.1016/j.lithos.2004.04.028.

Zedgenizov, D.A., Harte, B., Shatsky, V.S., Politov, A.A., Rylov, G.M., and Sobolev, N.V., and Edinburgh Ion Microprobe Facility (EIMF) (2006) Directional chemical variations in diamonds showing octahedral following cuboid growth. Contributions to Mineralogy and Petrology, 151, 45–57, https://doi.org/10.1007/s00410-005-0044-5.

Zedgenizov, D.A., Ragozin, A.L., Shatsky, V.S., Araujo, D., and Griffin, W.L. (2011) Fibrous diamonds from the placers of the northeastern Siberian Platform: Carbonate and silicate crystallization media. Russian Geology and Geophysics, 52, 1298–1309, https://doi.org/10.1016/j.rgg.2011.10.003.

Zedgenizov, D.A., Skuzovatov, S.Yu., Griffin, W.L., Pomazansky, B.S., Ragozin, A.L., and Kalinina, V.V. (2020) Diamond-forming HDFs tracking episodic mantle metasomatism beneath Nyurbinskaya kimberlite pipe (Siberian craton). Contributions to Mineralogy and Petrology, 175, 106, https://doi.org/10.1007/s00410-020-01743-8.

Manuscript received June 17, 2024
Manuscript accepted October 12, 2024
Accepted manuscript online October 22, 2024
Manuscript Handled by Oliver Tschauner

Endnotes:

[1]Deposit item AM-25-79503. Online Materials are free to all readers. Go online, via the table of contents or article view, and find the tab or link for supplemental materials.